
Masked Diffusion Models are Fast Learners

Jiachen Lei Peng Cheng Zhongjie Ba * Kui Ren

School of Cyber Science and Technology
Zhejiang University

Abstract

Diffusion models have emerged as the *de-facto* technique for image generation, yet they entail significant computational overhead, hindering the technique’s broader application in the research community. We propose a prior-based denoising training framework, the first to incorporate the pre-train and fine-tune paradigm into the diffusion model training process, which substantially improves training efficiency and shows potential in facilitating various downstream tasks. Our approach centers on masking a high proportion (e.g., up to 90%) of the input image and employing masked score matching to denoise the visible areas, thereby guiding the diffusion model to learn more salient features from training data as prior knowledge. By utilizing this masked learning process in a pre-training stage, we efficiently train the ViT-based diffusion model on CelebA-HQ 256×256 in the pixel space, achieving a 4x acceleration and enhancing the quality of generated images compared to DDPM. Moreover, our masked pre-training technique is universally applicable to various diffusion models that directly generate images in the pixel space and facilitates learning pre-trained models with excellent generalizability: a diffusion model pre-trained on VGGFace2 attains a 46% quality improvement through fine-tuning with merely 10% local data. Our code is available at <https://github.com/jiachenlei/maskdm>.

1 Introduction

Diffusion models or score-based models [54, 53, 25, 50, 30, 13] have emerged as the state-of-the-art technique in generative modeling, exhibiting remarkable performance in image synthesis. The denoising training, the core of the diffusion-based approach, has been quickly adopted in various domains such as image editing[46, 18, 2, 49], controllable image generation[41, 40, 47, 15, 39, 45, 11, 3], video synthesis[5, 27], and audio generation[57, 33]. These advancements have significantly contributed to the progress of generative modeling since the advent of generative adversarial networks (GAN)[19, 1, 48, 21], and diffusion models are taking over the predominating role of GAN-based methods[28, 29].

Although diffusion models demonstrate exceptional capability in image synthesis, they require intensive computational resources. As one type of likelihood-based generative model, diffusion models demonstrate strong mode-covering ability [43], which unfortunately makes them pay excessive attention to model the details of images. Consequently, these models require more training effort, particularly when dealing with high-resolution images [25].

While large-scale diffusion models such as Stable Diffusion[43] and DALL·E 2 [40] have achieved impressive results in high-resolution image synthesis, the significant computational resources and training overhead required for these models are affordable only to large organizations, severely prohibiting the accessibility of these generative technologies to broader research communities and audiences.

*Corresponding author



Figure 1: Samples generated by model that went through 200k steps pre-training and 20k steps fine-tuning on CelebA-HQ [29] 256x256, while the overall training expense is less than 3 V100-day

To alleviate the overall training expenses associated with diffusion models when trained on high-resolution images, we propose **Prior-Based Denoising Training**, a novel training framework incorporating prior learning into the denoising training process. Rather than directly approximating the target data distribution, we decompose the denoising process into two simple yet related training stages, creating a smooth and sequential learning path for diffusion models: the first stage, *masked pre-training*, masks parts of the input image and performs **Masked Score Matching (MSM)** on the visible parts, followed by *denoising fine-tuning* equipped with the conventional denoising score matching (DSM) objective[25, 55] as the second stage. Our key observation is that, when optimized through MSM, the model initially endeavors to approximate prominent features in the training data (such as the fundamental characteristics of a human face), thereby directing less attention toward subtle features that exhibit considerable variability and implicitly capturing prior knowledge of the distribution. In subsequent DSM, the model learns to capture more informative details and approximates training data distribution more stably and expeditiously. At last, the conventional sampling process can be applied to the trained model for image synthesis.

Our two-stage prior-based learning framework achieves substantial efficiency improvement in the diffusion process. Utilizing the framework, diffusion model training poses significantly less time overhead. Meanwhile, the trained models can generate high-quality images comparable to state-of-the-art methods. We demonstrate that our method could achieve approximately **4x acceleration** on convergence speed in comparison to DDPM on CelebA-HQ 256×256 .

In addition to reducing the training cost, the proposed framework exhibits other advantages. First, the proposed masked pre-training is a plug-and-play technique that can be combined with arbitrary denoising training algorithms. In this paper, we conduct experiments with vision transformer (ViT) [14] based network, UViT[4], within the context of DDPM. Still, our two-stage training framework can flexibly accelerate the denoising process for various diffusion model variants, e.g., diffusion models with CNN-based UNet[44] architectures or other denoising training frameworks [54, 53]. Second, the pre-trained model obtained from masked pre-training demonstrates excellent generalizability, benefiting a range of downstream tasks: 1) it efficiently reduces model training expenses in various downstream tasks; 2) it aids in fine-tuning diffusion models when facing limited training data. In certain privacy-sensitive applications, the pre-trained models present a lower risk of exposing sensitive training data (e.g., human faces) due to the masking strategy.

The **contributions** of our work can be summarized as follows:

- (i) To the best of our knowledge, we are the first to propose a prior-based denoising training framework that significantly reduces the cost of diffusion model training.
- (ii) We propose to incorporate pre-training and fine-tuning paradigms into the diffusion model training. In particular, we incorporate the masking strategy into the pre-training stage, forcing the diffusion model to learn prominent features from data. The pre-trained model expedites the following fine-tuning significantly and exhibits good generalizability for facilitating downstream tasks with limited data. In addition, we present a theoretical explanation of why masked training exhibits such advantages.

(iii) Our approach, compatible with arbitrary diffusion-based algorithms and network architecture, supports high-resolution image synthesis beyond the latent space. We conduct experiments to train ViT-based diffusion models using CelebA-HQ 256×256 in the pixel space, reducing the training cost to merely 25% of the baseline DDPM [25] while achieving better image generation. Moreover, our pre-trained model demonstrates excellent generalizability: by fine-tuning the pre-trained model with only 10% of local data, an improvement of 46% in the performance metric is observed for the downstream task.

2 Preliminary on Diffusion Models

Diffusion Models [50, 25] are latent variable models and are composed of a forward and a reverse process. The forward process is defined as a discrete Markov chain of length T : $q(\mathbf{x}_{1:T}|\mathbf{x}_0) = \prod_{t=1}^T q(\mathbf{x}_t|\mathbf{x}_{t-1})$. For each step $t \in [1, T]$ in the forward process, a diffusion model adds noise ϵ_t sampled from the standard Gaussian distribution $N(0, I)$ to data \mathbf{x}_{t-1} and obtains disturbed data \mathbf{x}_t from $q(\mathbf{x}_t|\mathbf{x}_{t-1}) = N(\mathbf{x}_t; \sqrt{1 - \beta_t}\mathbf{x}_{t-1}, \beta_t\mathbf{I})$. β determines the scale of added noise at each step and is prescribed such that $p(\mathbf{x}_T) \approx N(0, I)$.

Ho et al. [25] propose to use untrained linear β schedule where β_t increases linearly in the range of $[10^{-4}, 0.02]$. Later, Nichol et al. [36] introduce the cosine schedule to mitigate abrupt changes in noise level at $t = 0$ and $t = T$. Empirical evidence demonstrates that adopting the cosine schedule improves both the Negative Log-likelihood (NLL) and the sample quality of the diffusion model. Noticeably, instead of sampling sequentially along the Markov chain, we can sample x_t at any time step t in the closed form via $q(\mathbf{x}_t|\mathbf{x}_0) = N(\mathbf{x}_t; \sqrt{\bar{\alpha}_t}\mathbf{x}_0, (1 - \bar{\alpha}_t)I)$, where $\bar{\alpha}_t = \prod_{s=1}^t (1 - \beta_s)$.

The reverse process is also defined as a Markov chain: $p_\theta(\mathbf{x}_{0:T}) = p(\mathbf{x}_T) \prod_{t=1}^T p_\theta(\mathbf{x}_{t-1}|\mathbf{x}_t)$. In [25], $p_\theta(\mathbf{x}_{t-1}|\mathbf{x}_t)$ is parameterized as $N(\mathbf{x}_t; \mu_\theta(\mathbf{x}_t, t), \sigma_t)$, where $\mu_\theta(\mathbf{x}_t, t) = \frac{1}{\sqrt{\alpha_t}}(\mathbf{x}_t - \frac{\beta_t}{\sqrt{1-\bar{\alpha}_t}}\epsilon_\theta(\mathbf{x}_t, t))$ and σ_t is time dependent constant. ϵ_θ is parameterized by a neural network of which inputs are \mathbf{x}_t and time step t . Using this parameterization, the objective in [50] is simplified to:

$$L_{simple}(\theta) = \mathbb{E}_{t, \mathbf{x}_0, \epsilon} \left[\left\| \epsilon - \epsilon_\theta(\sqrt{\bar{\alpha}_t}\mathbf{x}_0 + \sqrt{1 - \bar{\alpha}_t}\epsilon, t) \right\|^2 \right] \quad (1)$$

As discussed in [54], the objective described in Eq.1 is essentially denoising score matching [55] and is the discretization of a particular continuous stochastic differential equation.

Subsequent to the training, samples are generated via iterating through the reverse process $p_\theta(\mathbf{x}_{0:T})$. Specifically, \mathbf{x}_T is first sampled from a standard Gaussian distribution $\mathcal{N}(0, \mathbf{I})$ and \mathbf{x}_t in each step is predicted as follows, where \mathbf{z} is sampled from a standard Gaussian distribution $\mathcal{N}(0, \mathbf{I})$.

$$\mathbf{x}_{t-1} = \frac{1}{\sqrt{\alpha_t}}(\mathbf{x}_t - \frac{1 - \alpha_t}{\sqrt{1 - \bar{\alpha}_t}}\epsilon_\theta(\mathbf{x}_t, t)) + \sigma_t\mathbf{z} \quad (2)$$

3 Prior-based Denoising Training

A diffusion model aims to learn the underlying distribution $p(\mathbf{x}_0)$ of actual data. Thereafter, samples could be easily drawn from the learned distribution following the sampling procedure. However, the training of diffusion models is time-consuming, and such impact aggravates intensively as the dimension of data distribution grows (e.g., high-resolution images). We propose to apply a two-step optimization to achieve efficient training: the first stage incorporates MSM to capture distribution priors. In the following step, the pre-trained model is optimized via the objective in Eq. 1 and can quickly approximate the true data distribution.

3.1 Key Insight

Our idea is inspired by the observation of the relationship between marginal and joint distribution. Consider an image denoted by $\mathbf{x}_0 = (x_0^1, x_0^2, x_0^3, \dots, x_0^N)^2$, where $\mathbf{x}_0 \in R^N$, and N represents the number of image pixels. Given a dataset of distribution $p(\mathbf{x}_0)$, which can be expressed as the joint distribution of N pixels, $p(\mathbf{x}_0) = p(x_0^1, x_0^2, x_0^3, \dots, x_0^N)$, our objective is to approximate the data distribution with $p_\theta(\mathbf{x}_0)$. Let τ represents a randomly selected subsequence of $[1, \dots, N]$

with a length of S . The marginal distribution of pixels, determined by τ , can be expressed as $p(\{x_0^{\tau_i}\}_{i=1}^S) = p(x_0^{\tau_1}, x_0^{\tau_2}, x_0^{\tau_3}, \dots, x_0^{\tau_S})$.

It is important to highlight that the distribution $p(\mathbf{x}_0)$ belongs to a family \mathcal{Q} of distributions that share the same set of $\binom{N}{S}$ possible marginal distributions $p(\{x_0^{\tau_i}\}_{i=1}^S)$. We introduce the term "marginal proxy distribution" to refer to any distribution in \mathcal{Q} other than $p(\mathbf{x}_0)$ that satisfies this condition. We represent such distributions using the notation $p_{\phi_S}(\mathbf{x}_0)$, where ϕ represents the parameters of the distribution and S specifies the length of the subsequence τ . Intuitively, the parameter S determines the degree of average similarity between the true data distribution and its marginal proxy distributions such that a higher value of S indicates a greater resemblance.

We demonstrate an example in the two-dimensional space. Assuming that we are approximating the Swiss roll distribution $p(\mathbf{x}_0)$, where $\mathbf{x}_0 = (x_0, y_0)$, Fig.2 displays a concrete example of the marginal proxy distribution $p_{\phi_1}(\mathbf{x}_0)$ in a blue heatmap which fully covers the Swiss roll data distribution (represented by the red line). Here, $S = 1$ implies that only a single component, x_0 or y_0 , is taken in a marginal distribution. $p_{\phi_1}(\mathbf{x}_0)$ shares the same marginal distribution $p(x_0)$ and $p(y_0)$ as the Swiss roll data while assuming independence between x_0 and y_0 such that $p_{\phi_1}(\mathbf{x}_0) = p(x_0)p(y_0)$. It is worth noting that there also exist other instances of $p_{\phi_1}(\mathbf{x}_0)$ that do not assume independence between x_0 and y_0 .

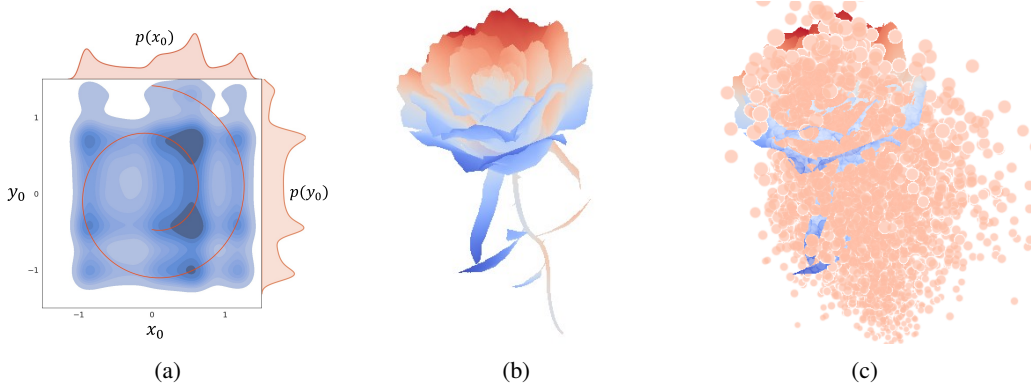


Figure 2: Toy example. (a) a 2D Swiss roll approximation example, where the red line is the Swiss roll distribution, the blue heatmap in the background is an instance of distribution $p_{\phi_1}(\mathbf{x}_0)$, and the top and right curve denote marginal distribution $p(x_0)$ and $p(y_0)$. (b) a 3D "rose" shape approximation example. (c) the rose is closely surrounded by 10k points that are sampled from the learned distribution $p_{\phi_2}(\mathbf{x}_0)$

When fitting either $p(x_0)$ or $p(y_0)$, both of which can be seen as multi-modal Gaussian distributions, we observe that approximating $p_{\phi_1}(\mathbf{x}_0)$ is comparatively easier than modeling the Swiss roll distribution $p(\mathbf{x}_0)$. Moreover, by leveraging the prior knowledge from $p_{\phi_1}(\mathbf{x}_0)$, we can efficiently approximate the true Swiss roll distribution instead of beginning from scratch. This is because $p_{\phi_1}(\mathbf{x}_0)$ fully covers the Swiss roll distribution, with the curve traversing most of its modes.

3.2 Overview

Motivated by the observations, we propose Prior-Based Denoising Training, which comprises two stages to approximate the data distribution $p(\mathbf{x}_0)$. In the first *masked pre-training* stage, we perform MSM to learn a marginal proxy distribution $p_{\phi_S}(\mathbf{x}_0)$ from the distribution family \mathcal{Q} that "encompasses" the true distribution. Since S is the important hyperparameter and the specific form of $p_{\phi_S}(\mathbf{x}_0)$ is not crucial for the training process, we implicitly approximate certain instances of $p_{\phi_S}(\mathbf{x}_0)$ by learning all possible marginal distributions $p(\{x_0^{\tau_i}\}_{i=1}^S)$ based on a randomly initialized neural network. In the second *denoising fine-tuning* stage, based on the learned prior $p_{\phi_S}(\mathbf{x}_0)$ from the first stage, we continue to estimate $p(\mathbf{x}_0)$ via the objective in Eq.1.

²We follow the conventions and denote a clean image as \mathbf{x}_0 , where the subscript 0 is the time step.

3.3 Masked Pre-training and Sampling

In this section, we formulate the objective function (i.e., MSM) in the masked pre-training, demonstrate the first stage’s training process, and further illustrate the sampling process of a model trained with our two-stage framework. We skip the introduction of the denoising fine-tuning since it is the same as the conventional denoising training process (see Section 2).

We approximate $p_{\phi_S}(\mathbf{x}_0)$ using a conditional diffusion model $p_{\theta}(\mathbf{x}_0|\tau)$, where the subsequence of pixels $\{x_0^{\tau_i}\}_{i=1}^S$ input into the model or the target marginal distribution is specified by τ . To achieve this, we employ a masking operation where we incorporate a randomly sampled sparse matrix $\mathbf{M} \in \{0, 1\}^{N \times N}$ and $\sum_{i=0}^N \mathbf{M}_{ij} = 1$, $\sum_{i,j} \mathbf{M}_{ij} = S$. As shown in Eq.3, this masking operation allows us to arbitrarily sample a subsequence $\{x_0^{\tau_i}\}_{i=1}^S$ from \mathbf{x}_0 .

$$\hat{\mathbf{x}}_0 = (\mathbf{x}_0 + \mathbf{H}) \cdot \mathbf{M} = \mathbf{x}_0 \cdot \mathbf{M} + \mathbf{H} \cdot \mathbf{M} \quad (3)$$

where $\mathbf{H} \in R^N$ can be represented as $\mathbf{H} = (h_1, h_2, \dots, h_N)$, and $\hat{\mathbf{x}}_0 = (x_0^{\tau_1} + h_{\tau_1}, x_0^{\tau_2} + h_{\tau_2}, x_0^{\tau_3} + h_{\tau_3}, \dots, x_0^{\tau_S} + h_{\tau_S})$. Each element of \mathbf{H} encodes the property (e.g., position) of the corresponding pixel x , which is known as positional embedding in vision transformer family[14, 34]. In this way, different combinations of pixels, specified by τ , are implicitly encoded in the corresponding subset of \mathbf{H} , allowing for the representation of possible marginal distributions. Meanwhile, the conditional model $p_{\theta}(\mathbf{x}_0|\tau)$ is converted into an unconditional one, $p_{\theta}(\hat{\mathbf{x}}_0)$, with the condition τ being merged with the model input. Consequently, the sampling of \mathbf{x}_t at any given time step can be expressed as: $\hat{\mathbf{x}}_t = \sqrt{\alpha_t} \hat{\mathbf{x}}_0 + \sqrt{1 - \alpha_t} \epsilon$. We optimize the following MSM objective:

$$L_{msm}(\theta) = \mathbb{E}_{t, \hat{\mathbf{x}}_0, \epsilon} \left[\left\| \epsilon - \epsilon_{\theta}(\sqrt{\alpha_t} \hat{\mathbf{x}}_0 + \sqrt{1 - \alpha_t} \epsilon, t) \right\|^2 \right] \quad (4)$$

The objective is formulated in a manner that exposes more similarity to the one used in Eq.1. Our method is agnostic to specific model architectures and we demonstrate the training together with sampling pipeline using a ViT-based backbone (see Fig.3 for illustration).

Training. Given an image $\mathbf{x}_0 \sim p(\mathbf{x}_0)$, our first step is to partition it into non-overlapping patches of size $p \times p$. Subsequently, we perform the masking operation in Eq.3 to all patches, retaining only visible ones, denoted as $\hat{\mathbf{x}}_0$. The visible patches are linearly mapped into tokens before element-wisely added with positional embedding. The number of visible patches, S , is predetermined and fixed throughout the training process. We will present further analysis on the influence of parameter S and the selection of \mathbf{M} in Section 4.2. The final step involves masked score matching on the visible patches to approximate the set of all possible distributions $p(\hat{\mathbf{x}}_0)$.

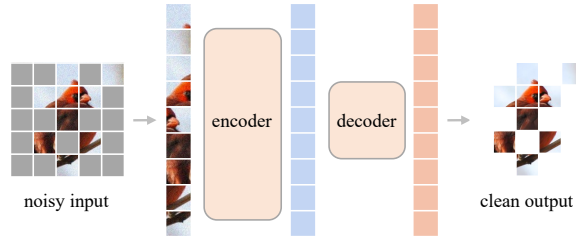


Figure 3: Illustration of the overall training process of masked diffusion model.

Sampling. We sample from $p_{\theta}(\hat{\mathbf{x}}_0)$ by setting \mathbf{M} as $\mathbf{1}$. Thereafter, following the procedure of DDPM in Eq.2, the sampling step is:

$$\hat{\mathbf{x}}_{t-1} = \frac{1}{\sqrt{\alpha_t}} \left(\hat{\mathbf{x}}_t - \frac{1 - \alpha_t}{\sqrt{1 - \alpha_t}} \epsilon_{\theta}(\hat{\mathbf{x}}_t, t) \right) + \sigma_t \mathbf{z}$$

In the context of 3-dimensional space, we present an example featuring an intricate target distribution resembling a rose flower. To effectively capture this distribution, we initially choose $S = 2$ and estimate the two-dimensional marginal distributions of the target distribution via MSM, specifically $p(x_0, y_0)$, $p(x_0, z_0)$, and $p(y_0, z_0)$. As shown in Fig.2, we observe that a learned marginal proxy distribution $p_{\phi_2}(\mathbf{x}_0) = p(x_0, y_0, z_0)$, fully encompasses the rose flower distribution. Leveraging the learned marginal prior $p_{\phi_2}(\mathbf{x}_0)$ as a favorable starting point, the model rapidly captures the actual distribution.

4 Experiments

In this section, we present three sets of experiments to evaluate the effectiveness and efficiency of prior-based denoising training. Firstly, we empirically identify the key factors influencing the masked score matching performance and determine the optimal configuration. In the second part, we conduct unconditional image synthesis to compare our approach with DDPM on commonly used benchmark datasets. Finally, we highlight the additional benefits enabled by our two-stage training paradigm. We validate the generalization capabilities of our pre-trained model in the transfer learning scenario.

4.1 Experimental Setup

Datasets. We mainly conduct key factor analysis and unconditional image synthesis experiments on two datasets, namely, CelebA [35] and CelebA-HQ [29]. CelebA consists of 200k training images featuring human faces. CelebA-HQ comprises 30k high-resolution human face images of size 1024×1024 and is produced by upsampling CelebA images with a neural network. We resize images from CelebA to 64×64 and images from CelebA-HQ to 256×256 . For the third set experiment, we show the benefits of masked pre-training under real-world transfer learning settings on VGGFace2 [7]. The dataset contains 3.31m face images of various resolutions featuring over 8.6k distinct identities within its training set.

Model	Depth	Dim	Heads	Params
MaskDM-S	12	512	8	44M
MaskDM-B	12	768	12	102M
MaskDM-L	16	1024	16	233M

Table 1: Details of models used in our experiments

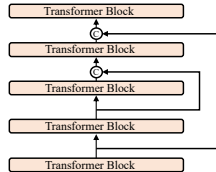


Figure 4: Encoder architecture of U-ViT

Architecture configurations. In our experiments, we employ three model configurations, with the parameter count ranging from 44 M to 233 M. These architectures are based on the ones proposed in [4], with certain modifications. Specifically, we utilize the U-ViT-Small setup from [4] as our MaskDM-S model, construct MaskDM-B by removing five transformer blocks from U-ViT-Mid to ensure efficient training on a single Tesla V100 GPU for one 256×256 image input, and derived our MaskDM-L model by making similar adjustments to U-ViT-Large. In all configurations, we adopt a single linear layer as the decoder and discard the convolutional block initially appearing in the U-ViT model. We utilize MaskDM-S for key factor study, employ MaskDM-L and MaskDM-B for unconditional image synthesis, and utilize MaskDM-S to validate the generalizability of masked pre-training. Further details regarding the configurations can be found in Tab.1.

Implementation details. Similar to the settings in [4], we conduct all experiments with mixed precision considering training efficiency, employ the AdamW optimizer with coefficients set to (0.99, 0.99), and adopt 0.03 weight decay on model parameters. We use a linear beta schedule in the key factor study and a cosine beta schedule in the rest experiments and set the maximum diffusion steps T to 1000. We maintain an exponential moving average (EMA) model with a decay of 0.999 during training and use the EMA model during sampling. Due to limited computing resources, we perform discrete wavelet transformation (DWT) in our unconditional image synthesis experiments to decompose the training images of CelebA-HQ, and the resulting spatial dimension of each DWT component becomes 128×128 . DWT processing is also applied to the baseline model for a fair comparison. Further detailed information is provided in the Appendix.

Computation resources. In the key factor analysis experiments, we train models using $2 \times V100$ GPUs. Besides, we train models using $8 \times V100$ GPUs in unconditional image synthesis experiments and $4 \times V100$ GPUs in experiments that verify the generalizability of the masked pre-training.

Evaluation. During the evaluation, we employ DDIM [51] to generate samples and present the FID-N score calculated between the generated samples and the entire training set. Fréchet Inception Distance (FID) [24] is the prevailing metric for measuring image quality, and the N in FID-N indicates the total number of generated images used for FID score computation.

4.2 Key Factor Analysis

We experimentally study the key factors of MSM to investigate the optimal configurations; then we provide empirical results to verify the unique benefits that masked pre-training can bring to the learning process.

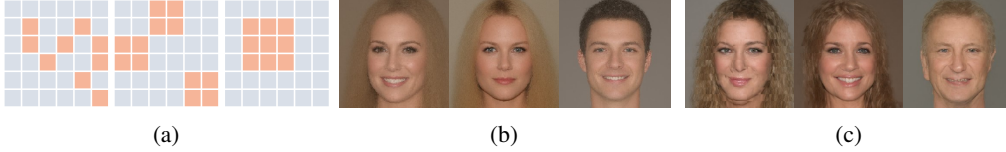


Figure 5: (a) Three mask types are examined in our experiments. From left to right, the mask types are represented as patch-wise masking, block-wise masking, and cropping. Samples in (b) and (c) are generated via masked pre-training on CelebA-HQ 256×256 , equipped with 90% patch-wise and block-wise masking, respectively. Notably, the model pre-trained with cropping at a 90% mask rate exhibits limited capability in generating plausible samples; therefore, we do not illustrate the results.

Mask Type and Mask Rate. We examine the impact of various masking techniques on MSM performance. Specifically, the vector M can be generated using patch-wise masking, block-wise masking, or cropping. The manifestation of each mask type is shown in Fig.5a: patch-wise masking entails the random occlusion of a predefined number of image patches, which retains information about the global structure. Block-wise masking involves randomly selecting image blocks for masking, where each block comprises a fixed quantity of image patches. It balances the information both from the local consistency and the global structure. Lastly, cropping entails randomly selecting a square region by determining its top-left coordinates and masking the area outside the chosen square. It mainly focuses on local consistency. In addition, we use mask rate m to describe the mask proportion, formulated as $m = 1 - \frac{S}{N}$, where S represents the subsequence length introduced in Section 3.3.

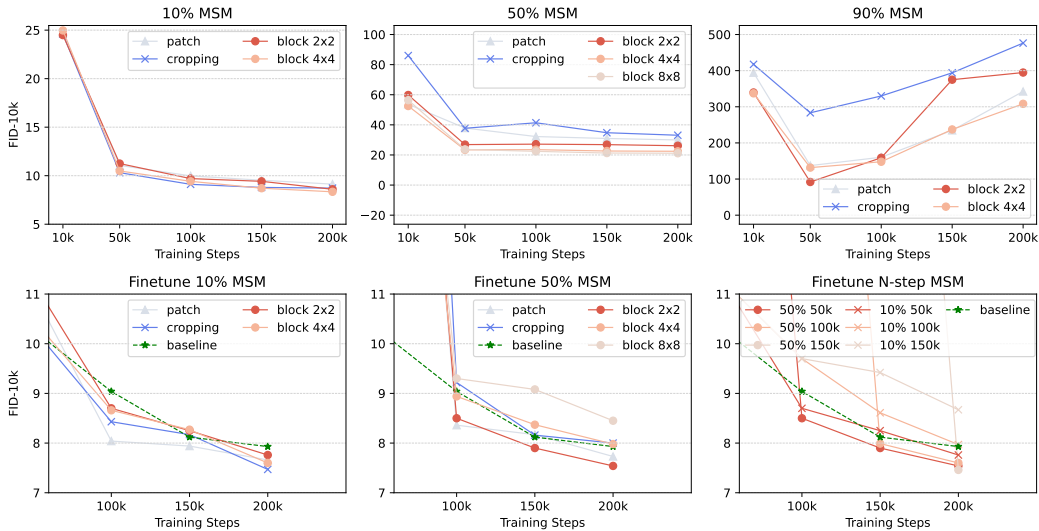


Figure 6: Empirical analysis on CelebA 64×64 . The experiments in the first row assess the efficacy of various mask types when optimizing with masked score matching, considering three different mask rates from left to right. In the second row, two experiments assess the efficacy of masked pre-training by evaluating the model’s performance post fine-tuning. Lastly, the experiment positioned at the bottom right examines the optimal training steps for block-wise masked pre-training. In the second row, we present the pre-training and fine-tuning FID scores sequentially in the same figure.

We analyze the performance of MSM under different combinations of mask rates and mask types. Specifically, models were trained using patch-wise masking, block-wise masking, and cropping at mask rates of 10%, 50%, and 90%, respectively. The first row of Fig.6 demonstrates that the models

trained under higher mask rates generally exhibit inferior FID scores compared to those trained with lower mask rates. A lower mask rate enables greater similarity between a marginal proxy distribution and the true data distribution, thereby yielding advantages in terms of FID score. Regarding the three mask types, cropping demonstrates marginally better performance under lower mask rates (e.g., $m = 10\%$), patch-wise masking only achieves intermediate performance, and block-wise masking consistently performs well across all experiments. Moreover, the study of different block sizes indicates that, when optimized with MSM, models consistently benefit from larger block sizes under low mask rates, while smaller block sizes prove more effective at higher mask rates (e.g., $m = 90\%$).

Hyperparameters. In experiments with 90% mask, we observe a rapid divergence of models after 50k training steps, while the FID scores in experiments with a 50% mask rate exhibit fluctuations. We hypothesize that a high mask rate leads to numerous possible combinations of marginal distributions, and the remaining image portion is insufficient, resulting in significant variance during the denoising training process. Consequently, the choice of hyperparameters plays a crucial role in the difficulty of training. Therefore, under 90% mask rate, we conduct further investigations into the impact of different hyperparameter configurations (e.g., learning rate, batch size, noise schedule, etc.), which is detailed in the Appendix. Experiments results validate that, among the hyperparameters, the noise schedule has more weight in affecting training stability. We can mitigate this instability and enhance the training process by selecting a more suitable schedule, such as the cosine schedule.

Benefits of Masked Pre-training. In this section, we investigate the advantages of masked pre-training in the complete two-stage diffusion training paradigm. We initiate the procedure by importing the weight parameters acquired from the MSM experiments concerning different configurations, such as mask type and rate. This entails leveraging a pre-trained model from the first stage. Then we fine-tune the model weights using the conventional denoising score matching described in Eq.1. In detail, our experiments utilize weights at 50k training iterations from scenarios with $m = 10\%$ and $m = 50\%$ configurations. The outcomes of this two-stage training process are illustrated in the left and middle subplots of the second row in Fig.6. We observe a positive correlation between the final performance of the two-stage training and that of the first stage (i.e., masked pre-training) models at the 50k training steps. However, for block-wise masking with a 50% mask rate, the ultimate performance tends to deteriorate as the block size increases, contrary to prior MSM experiments.

Cost of Masked Pre-training. In this study, we explore the optimal number of pre-training steps for 2×2 block-wise masking at 10% and 50% mask rates. We constrain the total number of training steps for prior-based denoising training to 200k steps and evaluate the overall performance of the two-stage learning approach with 50k, 100k, and 150k steps designated for masked pre-training. As illustrated in the rightmost subplot of the second row in Fig.6, the benefits of masked pre-training quickly diminish as the number of pre-training steps increases under a 10% mask rate. In contrast, for the 50% mask rate, the performance of masked pre-training stabilizes as the FID plateaus in previous MSM experiments.

Remarks. In conclusion, we argue that both local consistency and global structure information are pivotal factors in improving performance during the fine-tuning process. These factors are crucial priors requiring additional attention when approximating the marginal proxy distribution using MSM. Block-wise masking effectively provides both local consistency and global structure information concurrently, in contrast to patch-wise masking or cropping, which either emphasizes global structure and disregards local components or vice versa. Additionally, the relative importance of these priors is subject to the mask rate. By employing an appropriate mask rate and corresponding mask type, MSM could accelerate the convergence and augments the performance of diffusion models. In situations where the target distribution exhibits significant data dimensions, we recommend selecting a higher mask rate m during the first training step, alleviating challenges associated with approximating marginal proxy distributions $p_{\Phi_s}(\mathbf{x}_0)$ while maximizing the benefits brought by masked pre-training. In our experiments on CelebA 64×64 , block-wise masking emerges as a superior mask type and is suggested to be prioritized in various scenarios.

4.3 Unconditional Image Synthesis

In this section, we perform unconditional image synthesis experiments on CelebA-HQ 256×256 to assess the efficacy of our proposed prior-based denoising training method. During the first stage, the model is trained for 200k steps using a batch size of 128, with 4×4 block-wise masking at a 70% mask rate. Subsequently, we fine-tune the model weights from the final step of masked

pre-training, optimizing the denoising score matching objective (Eq.1) for 550k steps with a batch size of 16. For comparison, a baseline model is trained from scratch for 900k steps, employing identical hyperparameter settings as our two-stage approach and the same denoising objective used in the denoising fine-tuning stage.

Training acceleration. As illustrated in Fig.7, incorporating masked pre-training significantly enhances the performance of the vanilla DDPM. The left subplot of Fig.7 demonstrates that the model in pre-training achieves rapid convergence, with an FID-3K below 100 in just 50k steps. Building upon the pre-trained weights, the model in denoising fine-tuning attains an FID-3K score of nearly 20 in a mere 10k steps. Moreover, we significantly reduce the associated training costs compared to the baseline. Specifically, as illustrated in the right subplot of Fig.7, our approach attains an approximate $4\times$ **speedup** during the fine-tuning phase. We anticipate the acceleration effect to be further enhanced as the dimensionality of the data in the target distribution increases.

Performance comparison. We proceed to perform a comparative analysis with state-of-the-art approaches. Our chosen model MaskDM-L, trained under the above settings, employs 500-step DDIM sampling to generate 30k samples. Subsequently, we compute the FID using all generated samples while utilizing the entire training dataset as a reference. Meanwhile, we utilize the same sampling settings for the DDPM baseline and report the FID score of the model at 900k training steps. In comparison with existing methods, we utilize the FID scores reported in the respective papers. Specifically, we compare our method with DiffuseVAE [37] and Gen-ViT [58]. DiffuseVAE proposes a heterogeneous two-stage training method that concatenates the training procedures of variational autoencoder[31] and diffusion models. Gen-ViT explores the use of a single ViT for both image generation and classification, and it is one of the few ViT-based studies that report the performance of the ViT-based diffusion model on the CelebA-HQ 128×128 dataset. We argue the scarcity of employing ViT-based diffusion for high-dimensional image synthesis beyond latent space is due to training difficulty, which stems from the absence of the inductive bias within the ViT backbone and the computation complexity induced by the attention mechanism.

CelebA-HQ 128×128		
Method	FID ↓	Params
DiffuseVAE	10.87	116.3M
Gen-ViT	22.07	12.9M

CelebA-HQ 256×256		
Method	FID ↓	Params
DiffuseVAE	11.28	146M
DDPM Baseline	12.06	233M
MaskDM-B(ours)	10.77	102M
MaskDM-L(ours)	9.67	233M

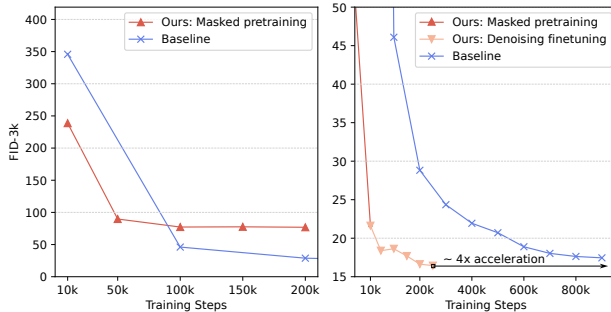


Table 2: Qualitative analysis

Figure 7: Convergence speed analysis

As shown in Tab.2, Gen-ViT [58] achieves FID of 22.07 on CelebA-HQ 128×128 , representing the challenges of training a ViT-based diffusion model to generate high-dimensional images. Additionally, it is notable that the number of Gen-ViT’s parameters is a mere 12.9 M, reflecting the difficulty associated with scaling up the model parameters, which poses a significant demand on computational resources such as GPU units. Regarding synthesizing 256×256 images, DiffuseVAE [37] reports an FID score of 11.28 with 146M parameters on CelebA-HQ 256×256 . Utilizing different batch sizes while keeping the rest hyperparameters similar as the MaskDM-L, we train MaskDM-B, a model with a comparable scale of parameters of DiffuseVAE, resulting in an FID score of 10.77 with fewer parameters after 2.81 V100-day pre-training and 24.3 V100-day fine-tuning. Furthermore, our MaskDM-L reaches an FID score of 9.67 after 10.9 V100-day pre-training and 23 V100-day fine-tuning. This performance surpasses the baseline model, which necessitates 32 V100-days of training, by a substantial margin while simultaneously requiring lower training costs.

Our primary goal is to achieve efficient diffusion training through prior learning using MSM. As such, we do not strive for the best FID performance once a satisfactory result is obtained, thus relaxing the pursuit of the FID score. Notably, it is promising to improve the metric further using advanced denoising training methods.

4.4 Generalizability

In addition to presenting an efficient training approach for image synthesis, we aim to provide a pre-trained model derived from the masked pre-training phase, facilitating seamless fine-tuning by other organizations using their proprietary data for diverse downstream tasks. To assess the feasibility, we investigate the generalizability of this pre-trained model. Our evaluation considers practical scenarios in real-world applications, accounting for data distribution shifts and varying amounts of data between the pre-training and downstream fine-tuning (i.e., the amount of local training data for downstream tasks is smaller).

We construct local training datasets comprising 10% and 1% of the CelebA-HQ 256×256 images and evaluate the performance of three models trained under distinct configurations. The baseline model employs score matching (Eq.1) for training from scratch on the limited data, taking 200k steps with a batch size of 64. In contrast, the other two models leverage weights pre-trained on the complete CelebA-HQ 256×256 and VGGFace2 256×256 datasets, respectively. The training process involves 200k iterations with a batch size of 256, leveraging 90% 4×4 block-wise masking. Subsequently, these pre-trained models undergo fine-tuning for 50k steps using the restricted local data. Despite the additional 50k training steps for the pre-trained models, their overall training cost remains significantly lower compared to the model trained from scratch, factoring in the pre-training expenses.

Training data	Baseline	Pre-trained on CelebA-HQ	Pre-trained on VGGFace2
10% data	37.17	24.59 (34% ↓)	20.71 (46% ↓)
1% data	63.33	32.51 (49% ↓)	36.51 (42% ↓)

Table 3: Generalizability of masked pre-training

Utilizing the **complete** CelebA-HQ 256×256 dataset as a reference, we present the FID-10k scores computed on samples generated through a 250-step DDIM evaluation. As demonstrated in Tab.3, masked pre-training can significantly enhance diffusion models’ performance. When only 10% of local data is accessible for training, the model pre-trained on the VGGFace2 256×256 dataset yields the best performance, exhibiting a 46% reduction in FID score compared to the baseline model. Meanwhile, the distribution approximated by the model pre-trained on CelebA-HQ 256×256 bears the highest resemblance to the 1% CelebA-HQ data distribution, achieving a 49% decrease in FID score. This finding suggests that a similar pre-training dataset is more advantageous when the available local training data is extremely limited. Additionally, our approach, which employs a high mask rate of up to 90%, offers significant advantages for privacy-sensitive situations in which the model publisher aims to minimize the risk of training data leakage.

5 Related Work

Efficient Training methods have drawn significant attention in generative modeling [9, 16, 10, 52, 26], and there is an urgent need for their application in the realm of diffusion models. The considerable training costs associated with diffusion models present an obstacle to entry and impede the advancement of the research community. To tackle this challenge, [43] proposes a novel approach that trains diffusion models in a low-dimensional latent space, thereby alleviating the burden on diffusion models to approximate extraneous details inherent in high-dimensional data. Another approach called MDT [17] employs masking in the training process of latent diffusion models. This method demonstrates improved efficiency based on the architecture proposed in DiT [6] for ImageNet 256×256 . However, MDT [17] is a one-stage training scheme exclusively designed for latent space training and could not benefit diffusion models trained in diverse settings. A concurrent but independent work proposes a similar approach, called patch diffusion [56], which masks the input image via cropping and trains the diffusion model following a stochastic masking schedule based on U-Net architecture. The method can be seen as a specialized instance of our method, where the architecture is CNN-based U-Net, and the mask type is chosen as cropping. Furthermore, our method could achieve significant training acceleration on CelebA-HQ 256×256 beyond the latent space compared to patch diffusion.

Vision Transformer (ViT) has revolutionized the field of various vision-related tasks. Recent research studies, such as [4, 38, 6], have incorporated ViT into diffusion model training by substituting the

prevalent CNN-based U-Net with more versatile ViT variants. These studies have empirically analyzed the factors that affect the quality of samples generated by ViT and proposed different strategies to address the challenges encountered in training ViT-based diffusion models.

Nonetheless, the predominant challenge in ViT-based diffusion models is the substantial computational burden, which includes high CUDA memory usage and lengthy training times. To mitigate these issues, ViT-based diffusion models are typically trained within the latent space (described in the Efficient Training part), given a high-dimensional data distribution (e.g., images $\geq 256 \times 256$). In this work, we propose masked score matching, which, for the first time, facilitates the training of ViT-based diffusion models on data beyond the latent space while preserving manageable computational expenses.

Pre-training plays a crucial role in visual discriminative tasks [42, 32, 22, 8] and has been widely studied. It is feasible to obtain a task-specific model by relying on a pre-trained model that is optimized with a surrogate objective, such as contrastive learning [20, 12, 23] or masked image modeling [22], which facilitates exceptional generalization capabilities. However, this two-stage training paradigm has received limited attention in the image generation domain. In this regard, we introduce the successful pre-train and fine-tune framework into denoising training, termed prior-based denoising training. Furthermore, we proposed masked score matching as the pre-training objective, which allows for acquiring an initial model that serves as a reasonable starting point for a wide range of downstream tasks in generative modeling.

6 Conclusion

This paper introduces prior-based diffusion training, a novel two-stage training framework that integrates pre-training into the diffusion training process for image generation models. Our approach substantially reduces the training cost while maintaining high image quality. Moreover, the framework’s first stage produces a surrogate model with strong generalization capabilities, enabling a wide range of downstream tasks. Applicable to all model architectures, including CNN and vision transformers, our training framework operates effectively beyond the latent space.

In the first pre-training stage, we propose masked score matching as the optimization objective and provide an intuitive theoretical foundation explaining the advantages of incorporating prior learning into the complete training process. We also explore various masking factors to determine the optimal masking strategies empirically. To demonstrate our method’s effectiveness, we conduct unconditional image synthesis using UViT on the pixel space, achieving capabilities better than a standard DDPM model while reducing training costs by 75%. In addition, we conduct experiments in realistic settings featuring distribution shifts and restricted data availability during fine-tuning to verify the generalizability of masked pre-training. The results demonstrate a notable improvement in the FID score. It is anticipated that our approach can be extended to various fields with diverse data modalities. Finally, we acknowledge the potential for a more appropriate pre-training objective to further improve the training of diffusion models, and we leave this exploration for our future work.

References

- [1] Martin Arjovsky, Soumith Chintala, and Léon Bottou. Wasserstein generative adversarial networks. In *International conference on machine learning*, pages 214–223. PMLR, 2017.
- [2] Omri Avrahami, Ohad Fried, and Dani Lischinski. Blended latent diffusion. *arXiv preprint arXiv:2206.02779*, 2022.
- [3] Yogesh Balaji, Seungjun Nah, Xun Huang, Arash Vahdat, Jiaming Song, Karsten Kreis, Miika Aittala, Timo Aila, Samuli Laine, Bryan Catanzaro, et al. ediffi: Text-to-image diffusion models with an ensemble of expert denoisers. *arXiv preprint arXiv:2211.01324*, 2022.
- [4] Fan Bao, Chongxuan Li, Yue Cao, and Jun Zhu. All are worth words: a vit backbone for score-based diffusion models. *arXiv preprint arXiv:2209.12152*, 2022.
- [5] Andreas Blattmann, Robin Rombach, Huan Ling, Tim Dockhorn, Seung Wook Kim, Sanja Fidler, and Karsten Kreis. Align your latents: High-resolution video synthesis with latent diffusion models. In *Proceedings of the IEEE/CVF Conference on Computer Vision and Pattern Recognition*, pages 22563–22575, 2023.

- [6] He Cao, Jianan Wang, Tianhe Ren, Xianbiao Qi, Yihao Chen, Yuan Yao, and Lei Zhang. Exploring vision transformers as diffusion learners. *arXiv preprint arXiv:2212.13771*, 2022.
- [7] Qiong Cao, Li Shen, Weidi Xie, Omkar M Parkhi, and Andrew Zisserman. Vggface2: A dataset for recognising faces across pose and age. In *2018 13th IEEE international conference on automatic face & gesture recognition (FG 2018)*, pages 67–74. IEEE, 2018.
- [8] Mathilde Caron, Hugo Touvron, Ishan Misra, Hervé Jégou, Julien Mairal, Piotr Bojanowski, and Armand Joulin. Emerging properties in self-supervised vision transformers. In *Proceedings of the IEEE/CVF international conference on computer vision*, pages 9650–9660, 2021.
- [9] Huiwen Chang, Han Zhang, Jarred Barber, AJ Maschinot, Jose Lezama, Lu Jiang, Ming-Hsuan Yang, Kevin Murphy, William T Freeman, Michael Rubinstein, et al. Muse: Text-to-image generation via masked generative transformers. *arXiv preprint arXiv:2301.00704*, 2023.
- [10] Huiwen Chang, Han Zhang, Lu Jiang, Ce Liu, and William T Freeman. Maskgit: Masked generative image transformer. In *Proceedings of the IEEE/CVF Conference on Computer Vision and Pattern Recognition*, pages 11315–11325, 2022.
- [11] Minghao Chen, Iro Laina, and Andrea Vedaldi. Training-free layout control with cross-attention guidance. *arXiv preprint arXiv:2304.03373*, 2023.
- [12] Xinlei Chen, Haoqi Fan, Ross Girshick, and Kaiming He. Improved baselines with momentum contrastive learning. *arXiv preprint arXiv:2003.04297*, 2020.
- [13] Prafulla Dhariwal and Alexander Nichol. Diffusion models beat gans on image synthesis. *Advances in Neural Information Processing Systems*, 34:8780–8794, 2021.
- [14] Alexey Dosovitskiy, Lucas Beyer, Alexander Kolesnikov, Dirk Weissenborn, Xiaohua Zhai, Thomas Unterthiner, Mostafa Dehghani, Matthias Minderer, Georg Heigold, Sylvain Gelly, et al. An image is worth 16x16 words: Transformers for image recognition at scale. *arXiv preprint arXiv:2010.11929*, 2020.
- [15] Dave Epstein, Allan Jabri, Ben Poole, Alexei A Efros, and Aleksander Holynski. Diffusion self-guidance for controllable image generation. *arXiv preprint arXiv:2306.00986*, 2023.
- [16] Patrick Esser, Robin Rombach, and Bjorn Ommer. Taming transformers for high-resolution image synthesis. In *Proceedings of the IEEE/CVF conference on computer vision and pattern recognition*, pages 12873–12883, 2021.
- [17] Shanghua Gao, Pan Zhou, Ming-Ming Cheng, and Shuicheng Yan. Masked diffusion transformer is a strong image synthesizer. *arXiv preprint arXiv:2303.14389*, 2023.
- [18] Vidit Goel, Elia Peruzzo, Yifan Jiang, Deja Xu, Nicu Sebe, Trevor Darrell, Zhangyang Wang, and Humphrey Shi. Pair-diffusion: Object-level image editing with structure-and-appearance paired diffusion models. *arXiv preprint arXiv:2303.17546*, 2023.
- [19] Ian Goodfellow, Jean Pouget-Abadie, Mehdi Mirza, Bing Xu, David Warde-Farley, Sherjil Ozair, Aaron Courville, and Yoshua Bengio. Generative adversarial nets. In Z. Ghahramani, M. Welling, C. Cortes, N. Lawrence, and K.Q. Weinberger, editors, *Advances in Neural Information Processing Systems*, volume 27. Curran Associates, Inc., 2014.
- [20] Jean-Bastien Grill, Florian Strub, Florent Altché, Corentin Tallec, Pierre Richemond, Elena Buchatskaya, Carl Doersch, Bernardo Avila Pires, Zhaohan Guo, Mohammad Gheshlaghi Azar, et al. Bootstrap your own latent-a new approach to self-supervised learning. *Advances in neural information processing systems*, 33:21271–21284, 2020.
- [21] Ishaan Gulrajani, Faruk Ahmed, Martin Arjovsky, Vincent Dumoulin, and Aaron C Courville. Improved training of wasserstein gans. *Advances in neural information processing systems*, 30, 2017.
- [22] Kaiming He, Xinlei Chen, Saining Xie, Yanghao Li, Piotr Dollár, and Ross Girshick. Masked autoencoders are scalable vision learners. In *Proceedings of the IEEE/CVF Conference on Computer Vision and Pattern Recognition*, pages 16000–16009, 2022.
- [23] Kaiming He, Haoqi Fan, Yuxin Wu, Saining Xie, and Ross Girshick. Momentum contrast for unsupervised visual representation learning. In *Proceedings of the IEEE/CVF conference on computer vision and pattern recognition*, pages 9729–9738, 2020.
- [24] Martin Heusel, Hubert Ramsauer, Thomas Unterthiner, Bernhard Nessler, and Sepp Hochreiter. Gans trained by a two time-scale update rule converge to a local nash equilibrium. *Advances in neural information processing systems*, 30, 2017.

- [25] Jonathan Ho, Ajay Jain, and Pieter Abbeel. Denoising diffusion probabilistic models. *Advances in Neural Information Processing Systems*, 33:6840–6851, 2020.
- [26] Jonathan Ho, Chitwan Saharia, William Chan, David J Fleet, Mohammad Norouzi, and Tim Salimans. Cascaded diffusion models for high fidelity image generation. *J. Mach. Learn. Res.*, 23(47):1–33, 2022.
- [27] Jonathan Ho, Tim Salimans, Alexey Gritsenko, William Chan, Mohammad Norouzi, and David J Fleet. Video diffusion models. *arXiv preprint arXiv:2204.03458*, 2022.
- [28] Phillip Isola, Jun-Yan Zhu, Tinghui Zhou, and Alexei A Efros. Image-to-image translation with conditional adversarial networks. In *Proceedings of the IEEE conference on computer vision and pattern recognition*, pages 1125–1134, 2017.
- [29] Tero Karras, Timo Aila, Samuli Laine, and Jaakko Lehtinen. Progressive growing of gans for improved quality, stability, and variation. *arXiv preprint arXiv:1710.10196*, 2017.
- [30] Tero Karras, Miika Aittala, Timo Aila, and Samuli Laine. Elucidating the design space of diffusion-based generative models. *arXiv preprint arXiv:2206.00364*, 2022.
- [31] Diederik P Kingma and Max Welling. Auto-encoding variational bayes. *arXiv preprint arXiv:1312.6114*, 2013.
- [32] Alexander Kirillov, Eric Mintun, Nikhila Ravi, Hanzi Mao, Chloe Rolland, Laura Gustafson, Tete Xiao, Spencer Whitehead, Alexander C Berg, Wan-Yen Lo, et al. Segment anything. *arXiv preprint arXiv:2304.02643*, 2023.
- [33] Haohe Liu, Zehua Chen, Yi Yuan, Xinhao Mei, Xubo Liu, Danilo Mandic, Wenwu Wang, and Mark D Plumbley. Audioldm: Text-to-audio generation with latent diffusion models. *arXiv preprint arXiv:2301.12503*, 2023.
- [34] Ze Liu, Yutong Lin, Yue Cao, Han Hu, Yixuan Wei, Zheng Zhang, Stephen Lin, and Baining Guo. Swin transformer: Hierarchical vision transformer using shifted windows. In *Proceedings of the IEEE/CVF international conference on computer vision*, pages 10012–10022, 2021.
- [35] Ziwei Liu, Ping Luo, Xiaogang Wang, and Xiaoou Tang. Deep learning face attributes in the wild. In *Proceedings of International Conference on Computer Vision (ICCV)*, December 2015.
- [36] Alexander Quinn Nichol and Prafulla Dhariwal. Improved denoising diffusion probabilistic models. In *International Conference on Machine Learning*, pages 8162–8171. PMLR, 2021.
- [37] Kushagra Pandey, Avideep Mukherjee, Piyush Rai, and Abhishek Kumar. Diffusevae: Efficient, controllable and high-fidelity generation from low-dimensional latents. *arXiv preprint arXiv:2201.00308*, 2022.
- [38] William Peebles and Saining Xie. Scalable diffusion models with transformers. *arXiv preprint arXiv:2212.09748*, 2022.
- [39] Zeju Qiu, Weiyang Liu, Haiwen Feng, Yuxuan Xue, Yao Feng, Zhen Liu, Dan Zhang, Adrian Weller, and Bernhard Schölkopf. Controlling text-to-image diffusion by orthogonal finetuning. *arXiv preprint arXiv:2306.07280*, 2023.
- [40] Aditya Ramesh, Prafulla Dhariwal, Alex Nichol, Casey Chu, and Mark Chen. Hierarchical text-conditional image generation with clip latents. *arXiv preprint arXiv:2204.06125*, 2022.
- [41] Aditya Ramesh, Mikhail Pavlov, Gabriel Goh, Scott Gray, Chelsea Voss, Alec Radford, Mark Chen, and Ilya Sutskever. Zero-shot text-to-image generation. In *International Conference on Machine Learning*, pages 8821–8831. PMLR, 2021.
- [42] Shaoqing Ren, Kaiming He, Ross Girshick, and Jian Sun. Faster r-cnn: Towards real-time object detection with region proposal networks. *Advances in neural information processing systems*, 28, 2015.
- [43] Robin Rombach, Andreas Blattmann, Dominik Lorenz, Patrick Esser, and Björn Ommer. High-resolution image synthesis with latent diffusion models. In *Proceedings of the IEEE/CVF Conference on Computer Vision and Pattern Recognition*, pages 10684–10695, 2022.
- [44] Olaf Ronneberger, Philipp Fischer, and Thomas Brox. U-net: Convolutional networks for biomedical image segmentation. In *International Conference on Medical image computing and computer-assisted intervention*, pages 234–241. Springer, 2015.

- [45] Nataniel Ruiz, Yuanzhen Li, Varun Jampani, Yael Pritch, Michael Rubinstein, and Kfir Aberman. Dreambooth: Fine tuning text-to-image diffusion models for subject-driven generation. In *Proceedings of the IEEE/CVF Conference on Computer Vision and Pattern Recognition*, pages 22500–22510, 2023.
- [46] Chitwan Saharia, William Chan, Huiwen Chang, Chris Lee, Jonathan Ho, Tim Salimans, David Fleet, and Mohammad Norouzi. Palette: Image-to-image diffusion models. In *ACM SIGGRAPH 2022 Conference Proceedings*, pages 1–10, 2022.
- [47] Chitwan Saharia, William Chan, Saurabh Saxena, Lala Li, Jay Whang, Emily L Denton, Kamyar Ghasemipour, Raphael Gontijo Lopes, Burcu Karagol Ayan, Tim Salimans, et al. Photorealistic text-to-image diffusion models with deep language understanding. *Advances in Neural Information Processing Systems*, 35:36479–36494, 2022.
- [48] Tim Salimans, Ian Goodfellow, Wojciech Zaremba, Vicki Cheung, Alec Radford, and Xi Chen. Improved techniques for training gans. *Advances in neural information processing systems*, 29, 2016.
- [49] Jaskirat Singh, Stephen Gould, and Liang Zheng. High-fidelity guided image synthesis with latent diffusion models. In *Proceedings of the IEEE/CVF Conference on Computer Vision and Pattern Recognition*, pages 5997–6006, 2023.
- [50] Jascha Sohl-Dickstein, Eric Weiss, Niru Maheswaranathan, and Surya Ganguli. Deep unsupervised learning using nonequilibrium thermodynamics. In *International Conference on Machine Learning*, pages 2256–2265. PMLR, 2015.
- [51] Jiaming Song, Chenlin Meng, and Stefano Ermon. Denoising diffusion implicit models. *arXiv preprint arXiv:2010.02502*, 2020.
- [52] Yang Song, Prafulla Dhariwal, Mark Chen, and Ilya Sutskever. Consistency models. *arXiv preprint arXiv:2303.01469*, 2023.
- [53] Yang Song and Stefano Ermon. Generative modeling by estimating gradients of the data distribution. *Advances in neural information processing systems*, 32, 2019.
- [54] Yang Song, Jascha Sohl-Dickstein, Diederik P Kingma, Abhishek Kumar, Stefano Ermon, and Ben Poole. Score-based generative modeling through stochastic differential equations. *arXiv preprint arXiv:2011.13456*, 2020.
- [55] Pascal Vincent. A connection between score matching and denoising autoencoders. *Neural computation*, 23(7):1661–1674, 2011.
- [56] Zhendong Wang, Yifan Jiang, Huangjie Zheng, Peihao Wang, Pengcheng He, Zhangyang Wang, Weizhu Chen, and Mingyuan Zhou. Patch diffusion: Faster and more data-efficient training of diffusion models. *arXiv preprint arXiv:2304.12526*, 2023.
- [57] Dongchao Yang, Jianwei Yu, Helin Wang, Wen Wang, Chao Weng, Yuexian Zou, and Dong Yu. Diffsound: Discrete diffusion model for text-to-sound generation. *IEEE/ACM Transactions on Audio, Speech, and Language Processing*, 2023.
- [58] Xiulong Yang, Sheng-Min Shih, Yinlin Fu, Xiaoting Zhao, and Shihao Ji. Your vit is secretly a hybrid discriminative-generative diffusion model. *arXiv preprint arXiv:2208.07791*, 2022.

A Additional Samples

A.1 Samples of model trained on CelebA-HQ 256×256

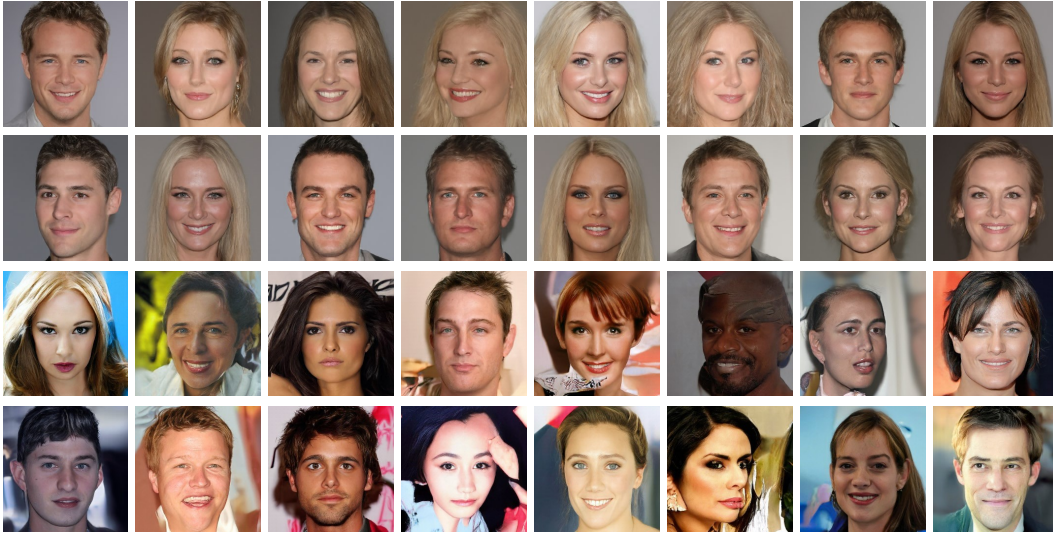


Figure 8: Uncurated samples of our MaskDM-L model reported in Tab.2. The first two rows contain samples generated by the model after 200k steps pre-training at a mask rate of 70%. The third and fourth rows contain samples generated by the model after 550k steps fine-tuning.

A.2 Samples of pre-trained model



Figure 9: Uncurated samples that generated by models that went through 90% 4×4 block-wise masked pre-training. The first two rows contain samples generated by model pre-trained on VGGFace2 256×256 . The third and fourth rows contain samples generated by model pre-trained on CelebA-HQ 256×256 .



Figure 10: Uncurated Samples that generated by models that pre-trained with 90% patch-wise masking for 200k steps on ImageNet-1K 256×256 , given images from a single category as training data. The first row displays samples from class n03788365 and the second row displays the samples generated by model pre-trained on it. The third row displays samples from class n01729322 and the fourth row displays the samples generated by model pre-trained on it.

A.3 Comparison to DDPM

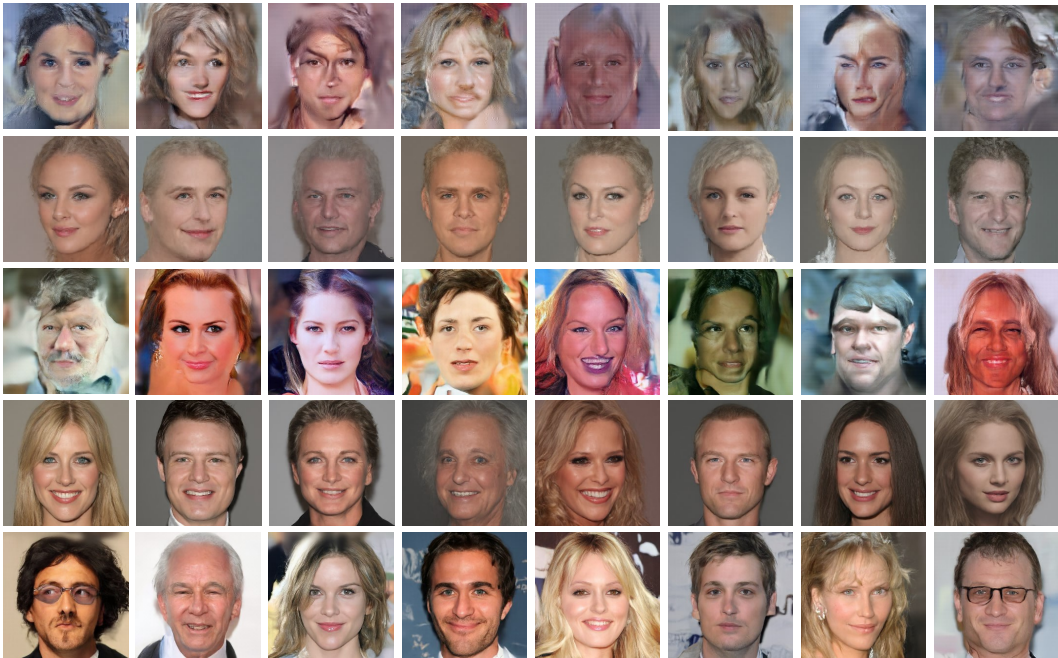


Figure 11: Comparison between samples generated by DDPM and our pre-trained model. The first and third rows display samples generated by DDPM models that are respectively trained for 50k steps and 200k steps. The second and the fourth rows display samples generated by our pre-trained models that are respectively trained for 50k steps and 200k steps. The last row displays samples generated by our model that is fine-tuned for 10k steps, subsequent to 200k pre-training.